Electrostatic Resonance-Cone Waves Emitted by a Dipole in the Ionosphere

H. Gordon James

***Abstract*—The theory of whistler-mode radiation from a dipole antenna has been tested in the ionospheric sounding-rocket experiment OEDIPUS-C (OC). In this bistatic investigation, 25-kHz waves were received at a distance of 1200 m from a synchronized transmitter. Electric fields near the group resonance cone were significantly stronger than in other directions, as predicted by theory. The transmitting antenna RF current was obtained from an equivalent circuit including an antenna impedance predicted by quasi-static theory. This current was applied to resonance-cone radiation theory. Observed radiated levels are about a hundred times greater than theoretical predictions based on some assumptions about the electromagnetics of the transmitting and receiving antennas. The modulation of the received signal caused by the spins of the transmitting and receiving dipoles was consistent with the electric field being polarized predominantly along the electrostatic wave-vector direction.**

***Index Terms*—Ionosphere, whistler-mode radiation.**

I. Introduction

INTEREST in active wave experiments in space plasmas dates from the early days of the space age. As soon as dependable RF equipment could be put into stable orbits, research on *in situ* and transionospheric propagation expanded considerably. Topside sounding [1] of the ionosphere from medium to high frequency (0.3–30 MHz) unveiled many features of the ionospheric structure. To this day, swept-frequency sounding remains in updated forms, a sought-after tool for local experiments on, and global images of, the ionosphere and magnetosphere. The launch on March 25, 2000 of the IMAGE spacecraft carrying a radio plasma imager [2] attests to this. The performance of sounder active dipoles, however, has not been widely studied. Research on topside-sounder observations has concentrated largely on the details of propagation in the ionosphere rather than on the injection of waves.

This paper presents some results from an ionospheric transmitter operating at 25 kHz. In the 1960s, active-wave research at very low frequency (VLF: 3–30 kHz) reflected communications goals of the times. The desire, then and since [3], for transionospheric communications provided a considerable impetus for the development of VLF propagation links using waves that could exit from the ionosphere the way natural whistlers do. The interest arose from the large skin depth of VLF waves in ocean water: it was realized that VLF waves from space could penetrate salt water and so provide a communications link to submerged submarines.

This led to a concerted theoretical work on active VLF dipoles and loops for the ionosphere. Arguably, the science story began with a theoretical treatment of the wave equation with external sources [4]. There followed about two decades of effort. Reference [5] includes a bibliography of this productive period.

Theoreticians have been attracted to the whistler mode in part by the mathematical challenge of its oblique resonance [6], [7]. The infinity in the cold-plasma dispersion relation at the oblique resonance is a mathematical singularity whose treatment is not intuitive and which requires some care. The oblique resonance turned out to be rather important for the radiated energy available from an antenna transmitting in the whistler mode.

Several spontaneous radio emissions of ionospheric or magnetospheric origin occur in the whistler mode. Consequently, there has also been some interest in *in situ* wave injection. In spite of several attempts since the 1970s to experiment expressly with active whistler-mode antennas in space, few have come to fruition [8], [9]. Evidence of resonant-cone far fields was produced at medium frequencies during fortuitous rendezvous of the ISIS-I and -II sounder satellites [10].

The whistler-mode resonance cone has been observed in the laboratory, in both the near field [11] and the radiation field [12], [13], and in the near field in space [14], [15]. The diagnostic possibilities of the resonance cone have also been investigated [16, refs. therein].

The 1995 flight of the sounding-rocket double payload OEDIPUS C (OC) yielded direct observations of both the near and radiated fields from a dipole in the whistler mode. An equivalent circuit analysis has been combined with dipole impedance theory to estimate antenna driving-point currents at 25 kHz. With the current established, this paper then proceeds to use published theories [17], [18] for the computation of the radiated far-field strengths, for comparison with the observations. The 25-kHz fields on the resonance cone are found to be about 100 times more intense than predicted by theory. The paper concludes with a discussion about factors that should be considered in the search for convergence of the theory and these observations.

II. RF Field Measurements at 25 kHz

The OEDIPUS-C (OC) sounding-rocket experiment [19] was launched at the Poker Flat Research Range in central Alaska at 06:38 UT on November 7, 1995. The rocket payload reached an apogee altitude of 824 km over northern Alaska about 8.6 min later. During the early part of this flight its forward and aft

Manuscript received June 29, 1999; revised May 22, 2000. The OEDIPUS-C experiment was a collaboration of the Canadian Space Agency and the National Aeronautics and Space Administration.

The author is with the Communications Research Centre, Ottawa, ON K2H 8S2, Canada (e-mail: gordon.james@crc.ca).

Publisher Item Identifier S 0018-926X(00)09378-9.

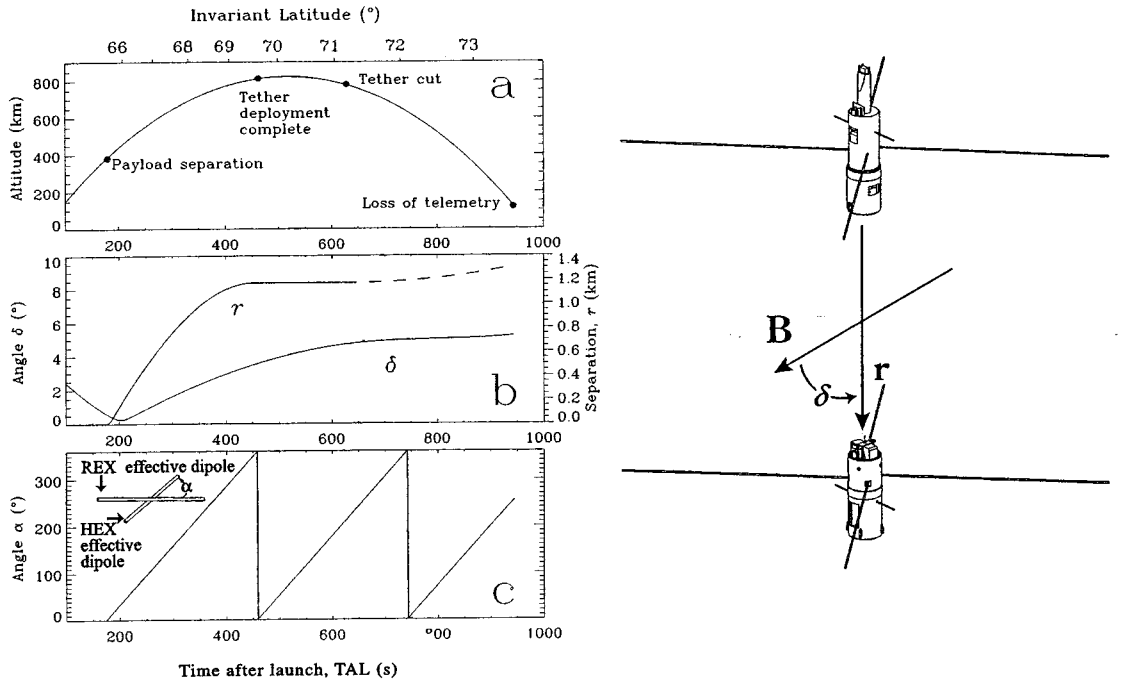

Fig. 1. (a) OC flight trajectory and significant events. (b) Histories of the magnitude r of the forward–aft separation $\mathbf{r}$ and of δ, the angle between $\mathbf{r}$ and $\mathbf{B}$, illustrated in the payload drawing on the right. The broken line after the time of tether cutting indicates that r is obtained from a calculation of the trajectories of the two subpayloads. (c) History of α, the relative total rotation of the forward dipole with respect to the aft dipole, modulo 360°.

subsections (subpayloads) were aligned with the magnetic field $\mathbf{B}$ and gradually separated as a 24-gauge conducting tether was unreeled between these two sections. Then, at about 1.8 min after apogee, the tether was cut at both ends in order to provide two free-flying subpayloads. The locations of the main events along the trajectory are shown in Fig. 1(a). Fig. 1(b) gives the histories of the angle δbetween the subpayload separation $\mathbf{r}$ and $\mathbf{B}$, and of the separation magnitude r. Similarly, Fig. 1(c) shows how the angle between the transmitting and receiving dipole axes changed with time [19].

A. Operational Modes of the OC Synchronized Transmitter–Receiver Pair

The forward OC subpayload contained a digitally controlled radio transmitter called the high-frequency exciter (HEX) and the aft subpayload contained a corresponding receiver for exciter (REX) which was tuned to the same frequency [19]. Both subpayloads had four tubular beryllium–copper monopoles forming a crossed dipole configuration. This geometry was required for spin stability of both subpayloads. The tip-to-tip length of each of the crossed-dipoles L or $2h$ was 19 m on HEX and 13 m on REX. The two terminals of the "V-dipole" antennas were the inner endpoints of two orthogonal monopoles. That is, pairs of adjacent orthogonal monopoles were connected together at the subpayload body to produce the "V" shape. The V dipole thus formed was considered equivalent to an effective linear dipole perpendicular to the magnetic field at both subpayloads. The axis of the effective linear dipole was assumed to lie along the bisectors of the Vs.

The subpayloads were programmed to commence separation at a time after launch (TAL) of 174 s. The separation occurred as planned at an altitude of 374 km on the trajectory up leg. This paper deals with two data intervals in the flight: the first 126 s after separation, during which r increased from 0 to 758 m; and then the principal observations after tether cutting at TAL $= 650 - 872$ s, during which separation went from 1175 m to 1252 m.

At zero separation, the HEX and REX dipoles were parallel. Both subpayloads were spin-stabilized along the $\mathbf{B}$ axis. The angle plotted in Fig. 1(c), panel 2(c) is the difference of the spin phases of the forward and aft effective dipole axes with respect to a celestial reference plane and gives a first-order indication of the actual angle between those two axes. The angle α increased linearly with time because the spin rate of the forward subpayload (0.088 Hz) was slightly greater than that of the aft subpayload (0.084 Hz). By the end of the first observation period at TAL $= 300$ s, the azimuth of the forward (HEX) dipole led that of the aft (REX) by 160°. During the second period, α went from 604° to 886°.

Observations at 25 kHz came from 0.5-s minor frames (MIFs) of the payload major-frame duty cycle. In these MIFs, the HEX was in its high-power (10 W) RF mode, and the HEX-REX pair operated synchronously in a pulsed swept-frequency mode SH3 [19], sweeping linearly in time from 25 kHz to 8.0 MHz in 50-kHz steps. The 25-kHz field data were recorded at the beginning of each sweep in a 50-kHz bandwidth, using a 600-s pulse followed by a 6-ms listening period. Higher frequency recordings during each sweep provided ionograms from which the ambient plasma frequency was scaled [19]. The HEX was off during another MIF using the SH3 sweep, permitting the REX to observe the background noise spectrum.

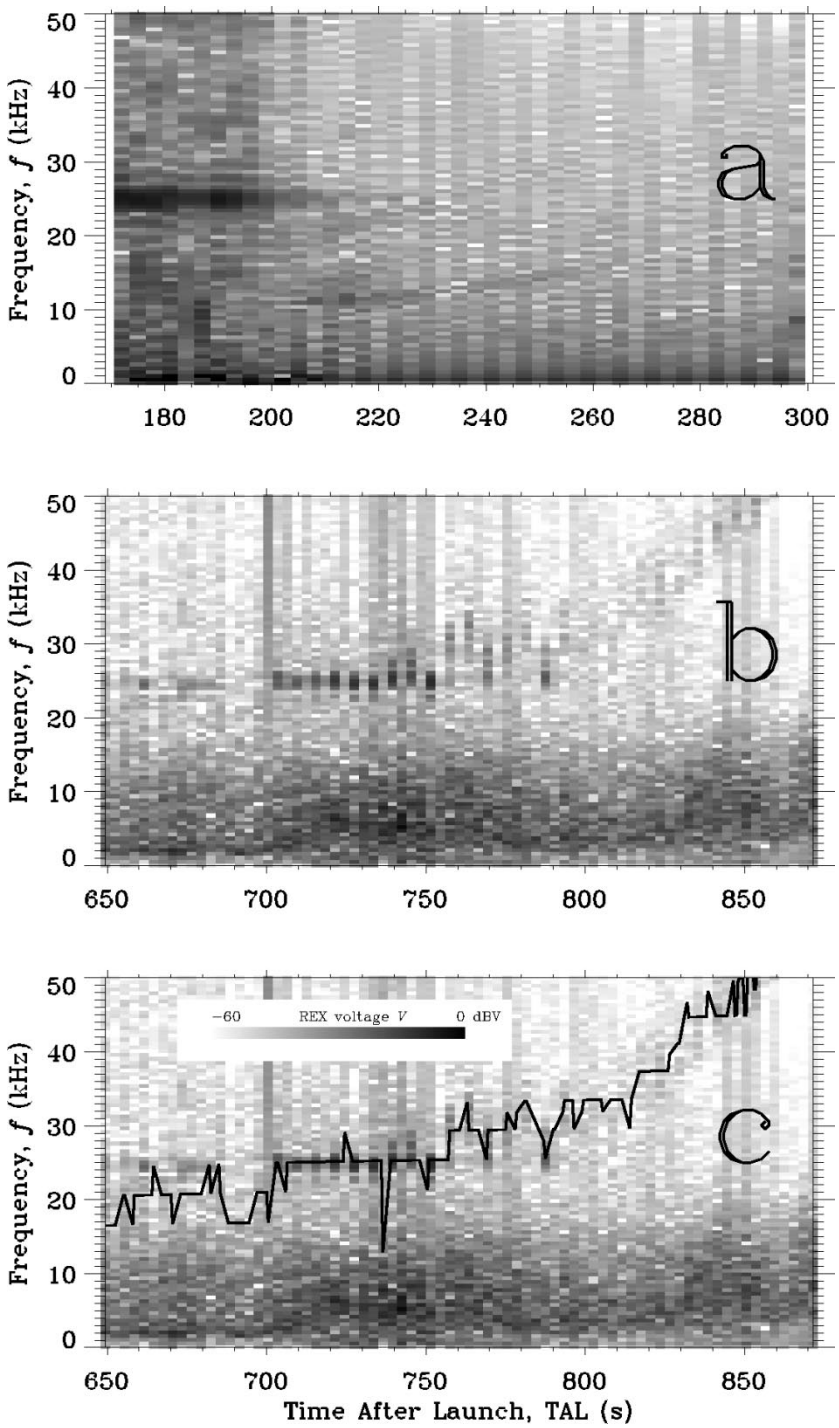

Fig. 2. Segments of the history of the spectrum of 25-kHz pulses. (a) Period TAL $= 171 - 300$ s, starting at HEX-REX turn-on time. (b) Period TAL $= 650 - 872$ s, following tether cutting. (c) Repeat of part b overlaid with predicted resonance cone frequency $f(t)$.

B. RF Voltages Observed by REX

Each panel in Fig. 2 contains a series of spectra of the signal voltage, for one of the two abovementioned periods of the flight. The spectra in Fig. 2 are of the RF voltage V at the REX-input antenna terminals. We show the results for the frequency bandwidth of primary interest 0–50 kHz. The blackness of the pixels is proportional to the spectral density of V^2, as indicated by the gradated scale in panel 2c. Fig. 2(a) covers the interval from HEX-REX turn-on at TAL $= 171$ s to TAL $= 300$ s. The main central lobe of the 25-kHz pulse spectrum stands above a broad spectrum distributed through all of the 0–50 kHz range. Both spectral components are from the HEX transmitter. Since the plasma frequency f_p varies from 850 to 350 kHz during the interval of Fig. 2(a) and since the cyclotron frequency f_c is about 1300 kHz, 25 kHz corresponds to the whistler mode. The whistler mode is the right-hand polarized cold-plasma mode occurring in regions 7 and 8 of the CMA diagram [7].

The thin rising feature on the left side of Fig. 2(a) starting at 10 kHz around 200 s is attributed to a tether coil resonance

stimulated by the HEX. As the tether is extended, the inductance of the tether remaining on the deployment reel changes, making the resonance frequency rise smoothly.

Fig. 2(b) contains the comparable grey-scale spectra of V^2 for the second period, 650–872 s. During the first part of this period, a clear HEX signal is seen near 25 kHz for about 100 s. The diffuse trace then rises in frequency over the next 100 s, going past the 50-kHz limit of the frequency scale at about 850 s. The data in Fig. 2(b) are the primary interest of this paper, and all come from one MIF in the major frame. They have essentially the same frequency-time signature as found in the other MIF in the major frame with 25-kHz measurements [20]. All of the signal frequencies in this event, from around 25 kHz through 50 kHz are known to be excited by the HEX because of its spectrum revealed in the close-in observations in Fig. 2(a) up to TAL $= 220$ s. With $0.2 < f_p < 1.0$ MHz and $1.16 < f_c < 1.38$ MHz at the payload during this second period, the frequencies 25–50 kHz continue to correspond to the whistler mode. A later section demonstrates how the resonance cone selects the frequency versus time signature in Fig. 2(b) and (c) and what can be learned about the dipole radiation efficiency at 25 kHz.

C. Near Fields of the Transmitting Dipoles

Quasi-static theory for the V-dipole impedance Z has been combined with a HEX circuit analysis to estimate the RF current into the transmitting dipole. The same technique for estimating I was used at 500 kHz [21]. An equivalent circuit of the HEX, its V-dipole and the impedance of the intervening electrical circuit in the forward subpayload is employed. It calls upon magnetoplasma dipole theory [22, eq. 64] to predict the dipole impedance. The theory provides impedance values in the neighborhood of $Z_d = 8100 - i55\,600\Omega$ for one of the crossed dipoles, forming the V and for the observed plasma parameters f_p and f_c values. The corresponding value of I is 5.4 mA for the rms driving-point current at the V-dipole terminals.

Consideration was given to scaling the dipole source currents from the amplitudes of near-field signals found in Fig. 2(a). Such fitting of the observed curves to near-field expressions for the electric dipole was used to obtain an independent estimate of I [21]. This procedure, however, appeared to have problems at 25 kHz. The geometry of the OC transmitting and receiving antennas with respect to the resonance cone indicates that the dipole lengths L are commensurate with the group resonance cone opening $s \approx 2r\tan\theta_{gr}$ in which $\tan^2\theta_{gr} = -S/P$, where S and P are elements of the dielectric tensor [7]. For instance, using $r = 100$ m, $f = 25$ kHz and the relevant plasma parameters for Fig. 2(a), $s \approx 2 \times 100 \times \tan 2.5^\circ = 8.7$ m. In comparison, the value of δ in Fig. 1(b) is 0.4° for $r = 100$ m, implying that the component of the separation of the HEX and REX perpendicular to $\mathbf{B}$ is only 0.7 m. Hence, out to $r = 100$ m, the REX dipole intersects the group resonance cones emanating from the HEX dipole. On account of the complicated intersection of the dipoles with resonant cone surfaces, quantitative use of near-field received voltages to determine I was not pursued.

D. Radiation Field Frequency-Time Signature Between 650 s and 850 s

The features of the signal are explained in terms of propagation near the resonance cone. First, as regards the shape of the frequency–time signature $f(t)$, the equality of the separation angle and the group resonance cone half-angle θ_{gr} [7] is

$$\tan^2\delta(t) = \tan^2\theta_{gr} = -\frac{S}{P} = \frac{-1+f_p^2(t)/\left(f(t)^2 - f_c^2(t)\right)}{1 - f_p^2(t)/f^2(t)}. \tag{1}$$

The t dependences take account of the geometry and plasma-parameter variations throughout the 200-s interval. Retaining only the extreme left and right sides of (1) gives a biquadratic in f, which yields the desired solution for $f(t)$

$$f(t) = \left[\frac{-B + (B^2 - 4AC)^{1/2}}{2A}\right]^{1/2} \tag{2}$$

where $A = -1 - \tan^2\delta$, $B = (1 + \tan^2\delta)(f_p^2 + f_c^2)$, and $C = -(\tan^2\delta)(f_p^2 + f_c^2)$. The plus sign is required in front of the round brackets in (2) for the lower oblique resonance cone. The OC ionograms provided the history of the ambient plasma frequency $f_p(t)$ [19], while $f_c(t)$ was computed using the IGRF1995 coefficients [23]. In the present study of the TAL period from 650 s to 850 s, where $f \ll f_p \ll f_c$ and θ_{gr} is about 5°, (1) and (2) simplify to

$$\theta_{gr} \approx \frac{f}{f_p}. \tag{3}$$

In Fig. 2(c), the resulting $f(t)$ curve is superposed on the spectral history of Fig. 2(b). The agreement between the calculated $f(t)$ locus and the observed signal enhancement is good throughout much of the 200-s duration. A number of the wide swings of the curve from pixel to pixel are reproduced particularly well between 750–800 s. It is thus concluded that the enhanced signal on the right side of Fig. 2(b) is simply the part of the broad transmitted spectrum that lies on the group resonance cone. The frequency evolves as shown because the changing circumstances dictate different frequencies that put the group resonance cone along the $\mathbf{r}$ direction. Fig. 2(c) confirms the theoretical prediction that the electric field is enhanced along the group resonance-cone direction.

III. Dipole Radiation Field

The field strength data of Fig. 2(b) are now compared with dipole theory. The radiation or far-field theory is used because the wavelengths of quasielectrostatic resonance cone waves are much smaller than the 1200 m separation of the HEX and REX. From relevant whistler-mode solutions of the complete hot-plasma electromagnetic dispersion relation [24], it is found that the value of the phase refractive index lies between about 30 and 1000 for propagation near the wave vector resonance-cone angle, θ_k. Given waves at 25 kHz, $\theta_k \approx 90^\circ - \theta_{gr} \approx 85^\circ$ and the corresponding wavelength range is 400 to 12 m.

The cold plasma theory predicts refractive indexes that become large without limit as the resonance cone is approached,

ruling out the use of such theory for predicting electric fields there. In the hot plasma theory and, in reality, fields are maximal but finite at the resonance cone, exhibiting interference fringes at directions inside the cone $\theta < \theta_{gr}$ [11], [14].

The electric field at and close to the whistler-mode resonance cone has been investigated theoretically for a dipole [17]. In spherical coordinates, this theory predicts θ and ϕ components in the E field

$$E_\theta = C_1 \cos\phi F''(\beta) \tag{4}$$

and

$$E_\phi = C_1 \frac{\sin\phi}{\sin\theta_{gr}} \left[\frac{\alpha^{1/2}\sin^2\theta_{gr}}{R}\right]^{2/3} F'(\beta) \tag{5}$$

in which

$$C_1 = \frac{(-i)^{2/3} IL\cos\theta_{gr}}{48\pi^2\varepsilon_0 f r^3 S}\left[\frac{\tan\theta_{gr}}{2\pi}\right]^{1/2}\left[\frac{R}{\alpha^{1/2}\sin^2\theta_{gr}}\right]^{5/3}$$

$$F(z) = \int_0^\infty \frac{dt}{t^{5/6}}\left(i^{2/3} z t^{1/3} - t\right)$$

$$\beta = \frac{R^{2/3}(\sin(\theta_{gr}-\theta)}{\alpha^{1/3}\sin^{4/3}\theta_{gr}}$$

α is a function of f, f_p and f_c, R is r divided by the electron gyroradius, I is the HEX input current and F' and F'' are the derivatives of the function F with respect to β. Fig. 3 sets out the geometry: the HEX is placed at the origin of a coordinate system and the REX at the position (r, θ, ϕ). The HEX dipole stays in the $x-z$ plane and $\mathbf{B}$ is along the z axis. The REX dipole is oriented along the direction x', which is specified with respect to the unit vectors $\mathbf{1}_r$, $\mathbf{1}_\theta$, $\mathbf{1}_\phi$, the directions of the components E_r, E_θ and E_ϕ, respectively. The payload attitude solution is used to determine the azimuth ϕ of the REX in the HEX-centered system, plus the angles ψ and η between the REX dipole axis x' and the E_θ and E_ϕ components, respectively.

Reference [17] predicts θ and ϕ components of the electric field $\mathbf{E}$, as shown in Fig. 4. E_θ is parallel to the quasi-electrostatic wave vector. Because the HEX subpayload spin keeps ξ values between $\pm 10°$, the theory for a perpendicular dipole is applied [17]. Except for ϕ values within a fraction of a degree of 90°, this theory predicts that the E_θ component is 10^3 times larger than the E_ϕ. The theory predicts that the phases of E_θ and E_ϕ vary in the E_θ direction with spatial periodicities λ of several meters. That is, λ is of the same order as the half length h. The θ value is assumed to center the REX dipole on the HEX group resonance cone, i.e., $\theta = \theta_{gr}$.

The HEX driving-point current I has been used as a fitting parameter throughout the subinterval 700–750 s, during which the signal was observed at frequencies close to 25 kHz. The voltage induced at the REX dipole is

$$V = \int_{-h}^{h} = [\cos\psi E_\theta(x'\cos\psi) + \cos\eta E_\phi(x'\cos\psi)]\,dx'$$

where the integral is evaluated along the dipole axis. This integral considers only the θ variation of E_θ and E_ϕ since the r and ϕ variations are negligible. The observed and theoretical $V(t)$ loci are compared in Fig. 5. A value of the driving-point current $I = 300$ mA is found to secure the best fit of the theory (broken line) to the observed V (solid line). This I value is impossible since the HEX can deliver only 108 mA into a matched load. The 300 mA value contrasts with the aforementioned estimate of 5.4 mA based on an impedance theory for the HEX dipole.

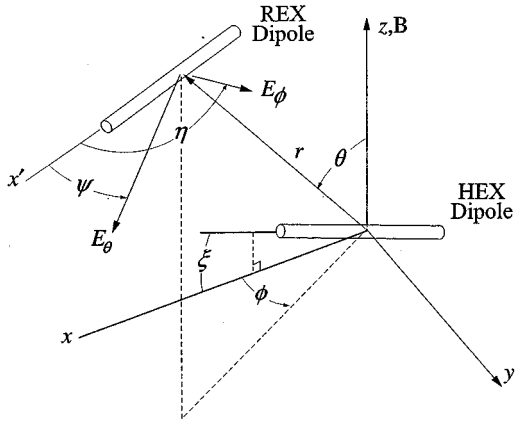

Fig. 3. Geometry of HEX and REX dipoles and the **E** field.

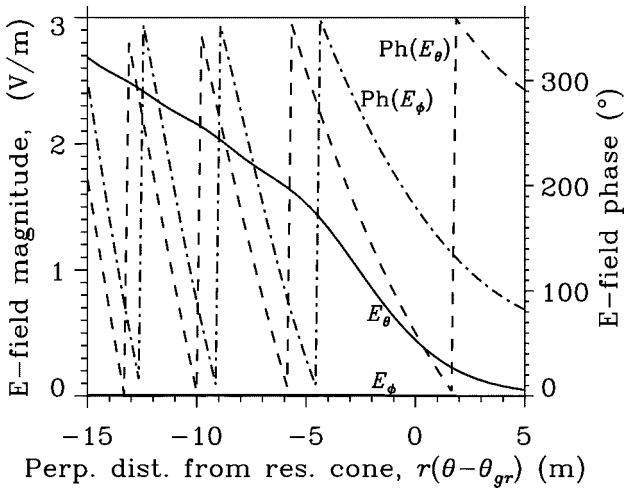

Fig. 4. Magnitude and phase of E_θ and E_ϕ as functions of the distance in E_θ direction, for $f = 0.025$, $f_p = 0.3$, $f_c = 1.2$ MHz, and $I = 1$ A.

In Fig. 5, the spin modulation is most pronounced during the period 700–750 s. This results from the fortuitous combination of two conditions: 1) the pixel separation in time 3 s is very close to one quarter of the subpayload spin period and 2) the extrema of ψ and ϕ happen to be in phase. The one-on/one-off pixel intensity modulation ensues, as seen in Fig. 2(b). Because ψ and ϕ equal 90° simultaneously, E_ϕ is found to contribute significantly to V at its minima.

The observed REX voltage $V_{\rm obs}$ in Fig. 5 diminishes abruptly at about 755 s. This is simply because this plot shows the voltage in the 25-kHz pixel. At 755 s, local f_p jumps upward forcing $f(t)$ upward also, and leaving little spectral power in the 25-kHz bin.

Reference [18] is a separate development of the electric potential in the vicinity of the whistler-mode group resonance cone for a short dipole. The point of departure is the same as in [17], the Poisson equation for a magnetoplasma in the quasi-static approximation. This work also takes account of warm-plasma contributions to the dispersion relation. Nevertheless, the resulting

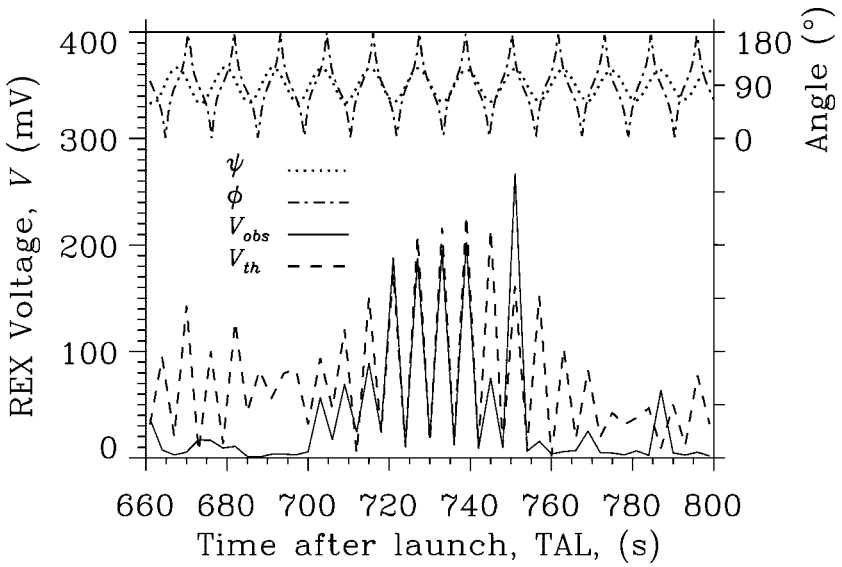

Fig. 5. Observed (solid line) and theoretical (broken line) received voltages V at 25 kHz. The observed pulse levels have been converted to equivalent CW levels to make them directly comparable with the CW theory. The theoretical values are calculated for $I = 300$ mA.

expression for the potential is dissimilar in the form of its dependence both on position coordinates and plasma parameters to the corresponding expression in [17]. This theory, too, predicts E-field values for $I = 5.4$ mA that are much lower than those observed at 25 kHz by OC.

IV. Discussion

A. Bounds on the Radiation Field

An unrealistically large value of driving-point current I is found necessary to make the theoretical E field agree with the observations. The following estimate of far electric field helps to substantiate the equivalent circuit estimate of I. The antenna impedance theory in the equivalent circuit analysis predicts a radiated power, $P = 0.14$ W. Ray directions are spread between 0° and a maximum angle $\theta_m = 14.8°$. If P were radiated isotropically inside a cone with this half-apical angle, the Poynting flux S_P at the median $r = 1185$ m would be $S_P = P/[4\pi r^2(1 - \cos\theta_m)] = 23.6\ \mu\text{Wm}^{-2}$. The corresponding rms electric field E would be $(2S_P/\epsilon_0 v_{gr})^{1/2}$. The cold-plasma group velocity is $v_{gr} \simeq$ c/1.3 for all θ except within about 5° of θ_{gr}. Applying this value of v_{gr}, one obtains $E \approx 15$ mV m^{-1}.

Dipole effective half lengths h_e to apply to the conversion of E to induced REX voltage $V = Eh_e$ might be as great as $2^{1/2}$ times the half length of the individual dipoles, making $h_e = 9.2$ m and $V = 140$ mV. In Fig. 5 peak voltages of about twice this value are observed during 720–740 s.

If radiated wavelengths near the resonance cone are small compared with h, then h_e, and hence V, may be overestimated. In addition, if the E fields near the resonance cone dominate those corresponding to wave vectors inside the cone, then one could find even lower electromagnetic power flux inside the cone. For these two additive effects, E values could be ten times higher on the resonance cone than at $\theta = 0$. This ratio appears reasonable in the light of similar values obtained in space [14], [15] and in laboratory [12]. Hence, the radiated fields deduced from rough energy considerations have better consistency with the observed radiated fields than those predicted by the detailed theory.

B. Pulse Spectra

The 25-kHz received pulses are found to be somewhat distorted from that of a pure rectangular 600-μs pulse. Selected individual power spectra of Fig. 2(a) and (b) are reproduced in Fig. 6(a)–(b), respectively. Fig. 6(a) gives the first 19 spectra after HEX-REX commence operation at TAL $= 171$, corresponding to the time from the left side of Fig. 2(a) up to 226 s. The first of the 19 successive spectra in Fig. 6(b) start at TAL $= 661$ and end at 715 s referred to Fig. 2(b). The irregularity of the sidelobe spacing and their peak values with respect to the main lobe show that the transmitted pulse is distorted with respect to a purely rectangular envelope of a 25 kHz carrier. The separations of the main lobe and the first spectral sidelobe in both frequency and level often exceed those expected for a rectangular pulse: 1.5/(600-μs) = 2.5 kHz and 13 dB, respectively.

Nevertheless, pulse distortion should not introduce a major error into the first-order analysis of radiated fields. The observed pulse levels, obtained from a Fourier analysis, have been converted to equivalent CW levels to make the spectral components directly comparable to the CW theory [17] in Fig. 5. The main spectral lobes in Fig. 6 have widths that are within 20% of the spectral widths of ideal square pulses. The absolute E-field analysis was based on the main lobes.

The spectra in Fig. 6 are useful in that they provide additional support for the foregoing statements about the relative strength of the resonance cone E field. First, consider the resolution of the spectra. By examining the partial derivatives of $f(t)$ in (3) with respect to the three independent variables δ, f_p and f_c, the largest uncertainty $\Delta f(t)$ is found to be $(\partial f/\partial f_p)\Delta f_p$. Plasma frequency values were scaled from the OC ionograms [19], which have a resolution of 50 kHz in the SH3 mode. This corresponds to $|\Delta f(t)| = 4000$ Hz. The fact that the signal maximum stays to within 1 pixel width, 521 Hz, throughout the

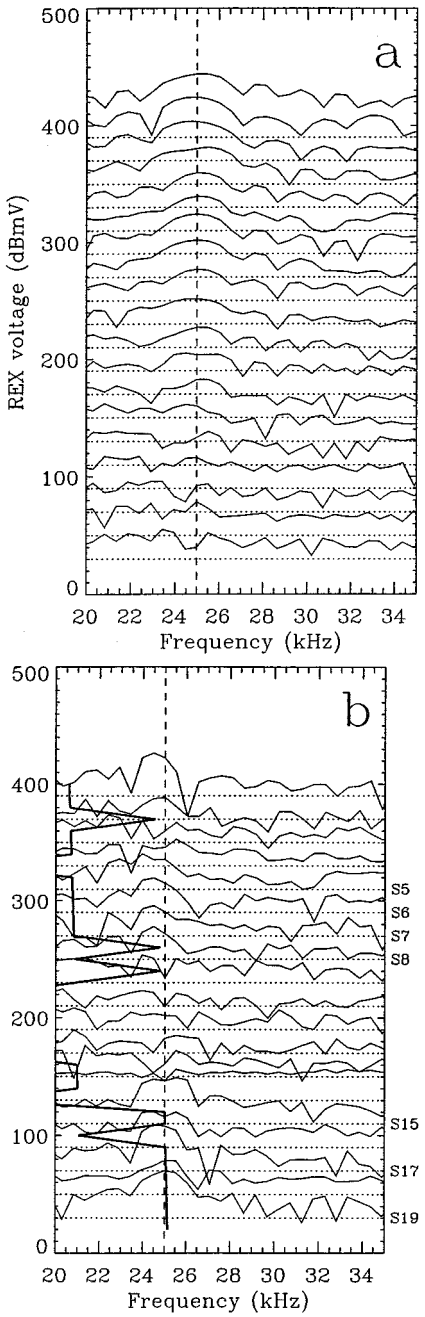

Fig. 6. Individual observed power spectra of 25-kHz pulses in solid line. The dotted lines are the 0-dBmV baselines for each succeeding spectrum, time increasing from the earliest spectrum at the top. (a) TAL $= 171 - 226$ s, starting just before subpayload separation. (b) TAL $= 661 - 715$ s. The heavier solid line is $f(t)$.

period 700–730 s means that the true f_p happens to stay much closer to the nominal scaled value of 0.3 MHz than can be measured. Hence, the central and first sidelobes of the 600-μs pulse spectrum separated by about 2.5 kHz are resolved. This allows one to proceed to a comparison of the intensities of spectral components on the resonance cone with those inside it.

The heavy line in Fig. 6(b) is the same as the heavy line in 2c, i.e., $f(t)$. The spectra in Fig. 6(b) most relevant to the comparison of field values on and inside the resonance cone are those with dotted baselines labeled "S5," "S6," "S7," and "S8." These spectra, from TAL $= 673 - -682$, exhibit weak peaks at 25 kHz and evidently occur when $f(t) \simeq 21$ kHz. This puts the observed 25-kHz component at a propagation angle inside the 25-kHz resonant k-cone. To find out how far inside the cone, it is first noted that the group resonance cone angle for $f = 25$ kHz with measured f_p centered around 0.250 MHz and $f_c = 1.17$ MHz is $\theta_{gr} = 5.8°$. The observed 25-kHz whistler-mode waves must have $\theta = \delta = 4.9°$. Hence, their group velocity direction is $\theta_{gr} - \theta = 0.9°$ away from the group cone.

The voltage values at 25 kHz in S6 through S8 are 26.7, 17.2 and 21.9 mV, respectively. These values are about one order of magnitude smaller than the 25-kHz peaks values between 720–750 s. To compare spectral intensities from the two periods, account must be taken of the dephasing of the angles $\psi(t)$ and $\phi(t)$ in the S6–S8 period. The signal levels during this period, 673–682 s, can be rendered comparable with the levels in 720–750 by multiplying by the ratio of the theoretical peaks in the same two periods. This is permissible because the theoretical modulation is determined solely by the changing orientation of the receiving dipole with respect to the assumed $\mathbf{E}$ vector direction. This compensation ratio is seen to be about 2. Compensating thus for angle, one finds again that the inside resonant-cone RF E fields are roughly one tenth of the most intense fields on the cone. This finding is not significantly affected with the realization that the E fields creating the S6–S8 spectra may not be linearly polarized as envisaged in Fig. 3. The absence of deep antenna spin modulation during the S5–S8 series of spectra means that the waves more likely have elliptic polarization, as expected in electromagnetic whistler-mode propagation.

Some features of the spectra between TAL $= 700$ s and 780 s in Fig. 2(b) and in other OC observations hint that the background auroral electron distribution may influence the strength of the transmitted 25-kHz signals. But the nature of the influence is not clear. Noise in the 0–15-kHz band is sustained throughout the figure, although it is slightly higher in 700–780 s than earlier or later. There are several isolated spectra in which strong noise stretches smoothly up to the highest frequency 50 kHz. The first clear case of such unexplained noise in Fig. 2(b) is at 700 s. OC data [25] show that the period 700–750 falls right between two regions of moderate field-aligned currents with opposite signs, each of about 2 μA m^{-2} peak magnitude.

C. Validity of Assumptions in the Theory

Given the conditions of the OC VLF transmission experiment, it does not constitute an ideal test of the theory [17], [18]. There are four concerns. First, in the basic electromagnetics of dipoles in anisotropic plasmas, it has not been demonstrated that the total field of the transmitting V dipole can be evaluated as the sum of two isolated dipoles at right angles. In addition, the axes of opposite monopoles in the both V antennas are not aligned; they are separated by 12 cm, suggesting that electric quadruple terms may contribute to the Green function. Another important assumption for review is that the received voltage can be found by a spatial integral of the radiated electric field in the absence of the receiving dipole.

Second, it has been assumed that the 1200 m separation of the REX and the HEX puts the former in the radiation zone of the latter. For lack of a plasma theory of near fields, suppose that the dependence of the electric field with r is that of a Hertzian

dipole. The ratio of the near field to the radiation field is then $1/(kr)^2$, where k is the wave number. With whistler-mode indexes of refraction between 30–1000, the ratio varies between about $15^{-2} - 500^{-2}$. This means that I would have to be between 225 and 25×10^4 larger to produce the observed E interpreted as a near field. The value 25×10^4 corresponds to waves nearest the resonance cone. All values between the two limits are in the opposite sense to what is needed to explain the Idiscrepancy. Hence, the use of far-field theories like those applied appears most reasonable.

A third concern is the possible distortion of the HEX radiated field by the free-flying tether wire. Immediately after tether cutting, the television on the aft subpayload showed the end of the freed tether receding from the subpayload along the r direction at a speed of the order of 1 ms^{-1}. Telemetry from the spool rotation sensor on the forward subpayload indicated that the associated pyrotechnic-driven guillotine had cut the wire there cleanly. As the post-tether-cut VLF experiment progressed, the wire shrank to a smaller overall dimension along r like a released coil spring. The coil resulted from the wire having been wound on the deployment spool, diameter $= 11.7$ cm.

If HEX fields had induced RF currents in the free-flying tether, one would have expected a reradiation pattern like that of a dipole aligned along $\mathbf{B}$. Theory [5], [17] predicts that the reradiation would be equally distributed through all magnetic azimuths about the wire. This fails to supply the concentration needed along $\mathbf{r}$ to explain the observed levels. Added to this is the fact that the HEX-radiated field near the group resonance cone are perpendicular to the cone. The important $\mathbf{E}$ fields are perpendicular to the wire, and thus not expected to induce large currents in it.

The possibility of direct excitation of tether-guided electromagnetic modes, such as sheath waves [26], at the near end of the tether is discounted. Tether guided modes require a radial $\boldsymbol{E}$ excitation, not the linear polarization of fields from the HEX dipole.

Fourth and finally, the previously mentioned pulse distortion may be interpreted as evidence for directly coupled antenna current and consequently for nonlinear effects in the antenna response. Probe theory for the HEX dipoles, instead of the quasi-static linear electromagnetic theory [22], in the equivalent circuit determination of I would help to establish whether this is an important possibility. In Fig. 2(b) notice how the transmitted signal begins to intensify again just before the $f(t)$ locus in 2c goes off scale at 50 kHz. This is possibly an evidence of second-harmonic nonlinear enhancement of the 25-kHz fundamental carrier wave form.

V. Conclusion

The OC HEX dipole radiates preferentially along the whistler-mode group resonance cone. The spin modulation of the received signal is consistent with the $\mathbf{E}$-field polarization being parallel to the electrostatic wave vector. The observed signal magnitudes require driving-point currents in the antenna theory that are unrealistically large. To address the latter finding, certain computational assumptions should be revisited, including: ignoring higher order terms than the dipole term in the multipole expansion of the total field; assuming the far-field conditions are met for all important wavelengths; representing both the transmitting and receiving V dipoles as effective linear dipoles; and putting the effective length of the receiving dipole equal to the physical tip-to-tip length in the V integral.

References

[1] "Special issue on topside sounding and the ionosphere," *Proc. IEEE*, vol. 30, pp. 859–1171, June 1969.

[2] B. W. Reinisch, D. M. Haines, K. Bibl, G. Cheney, J. A. Galkin, X. Huang, S. H. Myers, G. S. Sales, R. Benson, S. Fung, J. L. Green, S. Boardsen, W. L. Taylor, J.-L. Bougeret, R. Manning, N. Meyer-Vernet, M. Moncuquet, D. L. Carpenter, D. L. Gallagher, and P. Reiff, "The Radio Plasma Imager investigation on the IMAGE spacecraft," *Space Sci. Rev.*, vol. 91, pp. 319–359, Jan. 2000.

[3] 22 161P. R. Bannister, J. K. Harrison, C. C. Rupp, R. W. P. King, M. L. Cosmo, E. C. Lorenzini, C. J. Dyer, and M. D. Grossi, "Orbiting transmitter and antenna for spaceborne communications at ELF/VLF to submerged submarines," in *AGARD Conf. Proc. 529, ELF/VLF/LF Radio Propagation Syst. Aspects*. Springfield, VA: NTIS, 1993, pp. 33-1–33-14.

[4] F. V. Bunkin, "On radiation in anisotropic media," *Sov. Phys. JETP*, vol. 5, pp. 277–283, Sept. 1957.

[5] T. N. C. Wang and T. F. Bell, "VLF/ELF radiation patterns of arbitrarily oriented electric and magnetic dipoles in a cold lossless multicomponent magnetoplasma," *J. Geophys. Res.*, vol. 77, pp. 1174–1189, Mar. 1972.

[6] K. G. Budden, *The Propagation of Radio Waves—The Theory of Radio Waves of Low Power in the Ionosphere and Magnetosphere*. Cambridge, U.K.: Cambridge Univ. Press, 1985, p. 105.

[7] T. H. Stix, *Waves in Plasmas*. New York: American Inst. Phys., 1992, ch. 1–2.

[8] N. A. Armand, Yu. P. Semenov, B. Ye. Chertok, V. V. Migulin, V. V. Akindinov, V. I. Aksenov, G. V. Bashilov, P. M. Belousov, V. A. Blinov, E. P. Vyatkin, S. A. Gorbunov, S. M. Yermin, I. V. Lishin, D. S. Lukin, A. V. Moshkov, L. I. Nezhinskiy, V. G. Osipov, V. B. Presnyakov, A. E. Reznikov, Ye. A. Rudenchik, P. P. Savchenko, G. K. Sosulin, S. V. Sarostin, N. P. Chibinskiy, A. V. Shabanov, V. A. Shlykov, and I. N. Shugalev, "Experimental study of the radiation of a frame antenna, placed on the Mir-progress-28-Soyuz TM-2 orbiter complex, at very low frequencies in the Earth's ionosphere," *Sov. J. Commun. Technol. Electron.*, vol. 34, pp. 50–57, 1989.

[9] A. E. Reznikov, E. A. Rudenchik, and S. V. Sarostin, "VLF radiation generated by a loop antenna in the F2 layer of the ionosphere: Interpretation of the measurements," *J. Atmos. Terrestr. Phys.*, vol. 57, pp. 1299–1308, Sept. 1995.

[10] H. G. James, "Wave propagation experiments at medium frequencies between two ionospheric satellites: Whistler-mode pulses," *Radio Sci.*, vol. 13, pp. 543–558, May–June 1978.

[11] R. K. Fisher and R. Gould, "Resonance cones in the field pattern of a radio frequency probe in a warm anisotropic plasma," *Phys. Fluids*, vol. 14, pp. 857–867, Apr. 1971.

[12] R. W. Boswell, "Measurements of the far-field resonance cone for whistler mode waves in a magnetoplasma," *Nature*, vol. 258, no. 5530, pp. 58–60, Nov. 6, 1975.

[13] R. Stenzel, "Antenna radiation patterns in the whistler wave regime measured in a large laboratory plasma," *Radio Sci.*, vol. 11, pp. 1045–1056, Dec. 1976.

[14] A. Gonfalone, "Oblique resonances in the ionosphere," *Radio Sci.*, vol. 9, pp. 1159–1163, Dec. 1974.

[15] H. C. Koons, D. C. Pridmore-Brown, and D. A. McPherson, "Oblique resonances excited in the near field of a satellite-borne electric dipole antenna," *Radio Sci.*, vol. 9, pp. 541–545, May 1974.

[16] L. R. O. Storey, "Mutual-impedance techniques for space plasma measurements," in *Measurement Techniques in Space Plasmas. Fields*, R. F. Pfaff *et al.*, Eds. Washington, DC: American Geophys. Union, 1998, pp. 155–160.

[17] H. H. Kuehl, "Electric field and potential near the plasma resonance cone," *Phys. Fluids*, vol. 17, pp. 1275–1283, June 1974.

[18] E. A. Mareev and Yu. V. Chugunov, "Excitation of plasma resonance in a magnetoactive plasma by an external source. I. A source in a homogeneous plasma," *Radiophys. Quantum Electron.*, vol. 30, pp. 713–718, Aug. 1987.

[19] H. G. James and W. Calvert, "Interference fringes detected by OEDIPUS C," *Radio Sci.*, vol. 33, pp. 617–629, May–June 1988.

[20] H. G. James, "Whistler-mode radiation from a dipole," *Adv. Space Res.*, vol. 24, pp. 1073–1076, 1999.
[21] H. G. James, V. I. Sotnikov, W. J. Burke, and C. Y. Huang, "OEDIPUS-C observations of electrons accelerated by radio frequency fields at whistler-mode frequencies," *Phys. Plasmas*, vol. 6, pp. 4058–4069, Oct. 1999.
[22] K. G. Balmain, "The impedance of a short dipole antenna in a magnetoplasma," *IEEE Trans. Antennas Propagat.*, vol. AP-12, pp. 605–617, Sept. 1964.
[23] C. E. Barton, "Revision of the international geomagnetic reference field," *Eos Trans. AGU*, vol. 77, p. 153, Apr. 1996.
[24] H. G. James, "Whistler-mode hiss at low and medium frequencies in the dayside-cusp ionosphere," *J. Geophys. Res.*, vol. 78, pp. 4578–4599, Aug. 1973.
[25] P. Prikryl, H. G. James, D. J. Knudsen, S. C. Franchuk, H. C. Stenbaek-Nielsen, and D. D. Wallis, "OEDIPUS-C topside sounding of a structured auroral E region," *J. Geophys. Res.*, vol. 105, pp. 193–204, Jan. 2000.
[26] H. G. James, K. G. Balmain, C. C. Bantin, and G. W. Hulbert, "Sheath waves observed on OEDIPUS A," *Radio Sci.*, vol. 30, pp. 57–73, Jan. 1995.

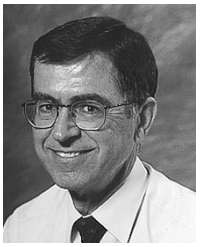

H. Gordon James received the B.Sc. degree in engineering physics from Queen's University, Kingston, ON, Canada, in 1963, and the M.Sc. and Ph.D. degrees in experimental plasma physics from the University of British Columbia, Canada, in 1965 and 1968, respectively.

From 1968 to 1970, he was a Research Associate at the Groupe de Recherches Ionosphériques, St-Maur-des-Fossés, France. There he studied VLF propagation in the FR-1 satellite program. Since 1970, he has been a Research Scientist in the Federal Government's Communications Research Centre, Ottawa, ON, Canada. Using data from satellites, rockets, and other sources, he has investigated spontaneous and artificial wave processes in the VLF to HF range. He has led the scientific planning of national and international radio-scientific experiments in space since the mid 1970s. From 1987, he has been the Principal Investigator for the Canadian Space Agency of the tethered rocket experiments OEDIPUS. His work has been concerned mainly with the physics of electromagnetic waves in the ionospheric plasma.

Dr. James is a Member of the Canadian Association of Physicists and the American Geophysical Union. He has served on advisory panels of the National Research Council of Canada, the Canadian Space Agency and the National Aeronautics and Space Adminstration (USA). He has been on the national executives of the Aeronomy and Space Physics Division of the Canadian Association of Physicists and the International Radio Science Union (URSI). He is currently URSI Commission H Chairman.